MODELLING ATTENUATION OF IRREGULAR WAVE FIELDS BY ARTIFICIAL ICE FLOES IN THE LABORATORY

A PREPRINT

A. Toffoli
The University of Melbourne, 3010 Vic., Australia
toffoli.alessandro@gmail.com

J.P.A. Pitt
University of Adelaide, 5005 S.A., Australia

A. Alberello
University of East Anglia, NR4 7TJ, United Kingdom

L.G. Bennetts
University of Adelaide, 5005 S.A., Australia

September 13, 2022

ABSTRACT

A summary is given on the utility of laboratory experiments for gaining understanding of wave attenuation in the marginal ice zone, as a complement to field observations, theory and numerical models. It is noted that most results to date are for regular incident waves, which, combined with the highly nonlinear wave-floe interaction phenomena observed and measured during experimental tests, implies the attenuation of regular waves cannot necessarily be used to infer the attenuation of irregular waves. Two experiments are revisited in which irregular wave tests were conducted but not previously reported, one involving a single floe and the other a large number of floes, and the transmission for the irregular and regular wave tests are compared. The transmission spectra derived from the irregular wave tests agree with the regular wave data, but are overpredicted by linear models due to nonlinear dissipative processes, regardless of floe configuration.

1 Introduction

Ocean waves are a defining component of the marginal ice zone (MIZ) Squire et al. [1995], Squire [2011], Williams et al. [2013a,b], Brouwer et al. [2021]. They regulate floe sizes and ice dynamics Alberello et al. [2020], Williams et al. [2017] in the MIZ, and hence ice extent and volume Bennetts et al. [2017] (see also the reviews Horvat [2022], Dumont [2022] in this issue). The ability to predict wave evolution in the MIZ, particularly wave attenuation over distance, is crucial to model wave-driven processes, such as ice breakup, and, hence, inform climate studies, evaluate ecosystem adaptation to climate change and plan exploitation of natural resources in polar regions Thomson [2022]. Field campaigns are critical to understand and model fundamental physics, but the harsh MIZ environment makes in-situ observations challenging Kohout et al. [2014], Thomson and Rogers [2014], Vichi et al. [2019], Kohout et al. [2020], Alberello et al. [2022]. As a complement or an alternative, laboratory experiments can be used to model complex ocean processes under controlled conditions, even in extreme sea states Onorato et al. [2009].

Laboratory experiments have a long tradition in the field of marine hydrodynamics, typically using model ice (saline or doped; see Riska [2018]). They have only relatively recently started being used to investigate wave-floe interactions and wave propagation in the MIZ, to evaluate wave attenuation (and closely related wave transmission) Wang and Shen [2010], Alberello et al. [2021] and concurrent wave forcing on floes, e.g. breakup Dolatshah et al. [2018], Passerotti et al. [2022] and rafting Dai et al. [2004]. The majority of laboratory experiments on wave propagation in the MIZ employ artificial ice floes (e.g. plastic plates), as they are more versatile, e.g. do not require an ice tank and are easier to attach instruments to, while also providing a more compliant elastic response than model ice, which exhibits unwanted plastic behaviour von Bock Und Polach et al. [2021].

The laboratory experiments are often used to assess predictions given by theoretical models of wave-floe interactions and wave propagation in the MIZ. Use of artificial floes in the experiments is consistent with theoretical model assumptions

in the so-called scattering regime, where floes are typically modelled as thin elastic plates when wavelengths (L_w) are shorter than floe lengths (L_f) and, hence, floes flex in response to wave forcing Peter et al. [2004], Bennetts and Williams [2010], Montiel et al. [2013b,a], Meylan et al. [2015a], or rigid bodies when wavelengths are greater than floe lengths Masson and LeBlond [1989], Meylan et al. [2015b], Yiew et al. [2016], Orzech et al. [2016], McGovern and Bai [2014], Bai et al. [2017]. Scattering is negligible for wavelengths much greater than floe lengths ($L_w/L_f \gg 1$), and the floes are usually treated in theory as a continuum, resulting in a dispersion relation where, in contrast to energy-conserving scattering models, attenuation is created by a dissipative process Meylan et al. [2018], Golden et al. [2020], H. [2022], which makes the validity of artificial floes less clear. Almost all theoretical models are linear, i.e. results scale linearly with the incident wave amplitude on the basis of small steepness ($\varepsilon = \pi H/L_w$, where H is the wave height), and treated in the frequency domain with regular incident waves.

For the sake of consistency with theoretical models and for simplicity, almost all laboratory experiments use regular incident waves. For instance, Bennetts et al. [2015] analysed transmission of regular waves by a single square plastic floe in a wave basin. They found the transmitted wave field becomes irregular for large incident steepnesses and the transmission coefficient (i.e. the proportion of incident energy transmitted) tends to decrease with increasing steepness. They attributed the irregularity to the steeper incident waves (i) causing the floe to slam against the water surface and (ii) forcing water onto the upper floe surfaces due to their small freeboards, in a process known as overwash Meylan et al. [2015a], Skene et al. [2015], thus creating high-frequency transmitted wave components. Moreover, they hypothesised that energy dissipation due to overwash and slamming reduces transmission, where the former was backed by a negative correlation between transmission coefficients and overwash depths.

Toffoli et al. [2015] used measurements of reflection and transmission in wave flume experimental tests to show incident wave energy is dissipated during interactions with the floe and that the proportion of dissipation increases with increasing steepness. Nelli et al. [2017] extended the study to a wider range of tests, and compared with tests where edge barriers were attached to the floe to prevent overwash, for which it was found that negligible wave energy is dissipated. Subsequent numerical modelling Nelli et al. [2020] and theory Skene and Bennetts [2021] gives further support that overwash results in wave energy dissipation.

Bennetts and Williams [2015] studied wave transmission through an array of circular wooden floes in a large wave basin. Tests were conducted for a low-concentration array involving 40 well-separated floes, and a high-concentration array involving 80 densely-packed floes. For the low-concentration array, linear attenuation models Meylan et al. [1997], Bennetts and Squire [2012] were shown to predict transmission accurately for gentle incident waves (generally $\varepsilon \leq 0.1$) over $L_w/L_f = 0.6$–6.3. Larger steepness waves were tested at two wavelengths, and, for the shorter wavelength, the larger steepness caused the transmission coefficient to decrease by 13%. The decrease was attributed to deeper and more energetic overwash, which was observed but not measured during the tests. For the high-concentration array, the linear model was shown to overpredict transmission, particularly for mid-range wavelengths, which was attributed to the strength and frequency of floe-floe collisions forced by the incident waves, and backed by analysis of accelerometer measurements on a subset of the floes. The finding has motivated subsequent experimental and numerical studies of wave-induced floe–floe collision properties Yiew et al. [2017] and their contribution to wave attenuation Herman et al. [2019].

Ocean waves, such as those that propagate through the MIZ, are irregular, and typically modelled as a superposition of regular components with random phases and different amplitudes, wavelengths and directions Onorato et al. [2009]. For linear systems, the regular wave components can be superposed to form the response for irregular wave forcing. However, the regular wave experiments discussed above indicate the nonlinear processes of overwash, collisions and slamming occur in wave-floe interactions, even for relatively small incident steepness waves for which linear theory would usually be considered valid. Therefore, in this article, we revisit the experimental campaigns of Bennetts et al. [2015], Bennetts and Williams [2015], and analyse previously unreported tests involving irregular incident waves. We compare transmission for the regular and irregular tests, with a particular focus on the influence of nonlinear wave-ice interaction processes.

2 Single floe experiments

2.1 Experimental set-up

An experiment was conducted in the wave basin at the Coastal Ocean And Sediment Transport laboratories of the University of Plymouth, UK. The basin is $10\,$m wide, $15.5\,$m long and was filled with fresh water $0.5\,$m deep (Fig. 1a). At one end of the basin, a wave-maker with 20 individually controlled active pistons generated incident waves. The pistons automatically adjust their velocities to absorb waves reflected by side walls or the floe. At the other end, a sandy beach with a 1:10 linear slope dissipated about 95% of the incoming wave energy (standard for linear profiles, e.g.

Dolatshah et al. [2018], Onorato et al. [2009]). Residual energy returning from the beach is absorbed by the active pistons, preventing the formation of persistent oscillations in the basin.

A square polypropylene floe with side lengths $L_f = 1$ m and thickness 5 mm was deployed 2 m from the wave-maker (Fig. 1a). Its density of $905\,\mathrm{kg\,m^{-3}}$ and Young's modulus of 1.6 GPa are comparable to sea ice, which has density varying from 720–940 $\mathrm{kg\,m^{-3}}$ and Young's modulus from 1–6 GPa Timco and Weeks [2010] (no scaling factor is applied). The high density allows a small freeboard, facilitating overwash (Figs. 1b,d) even in mild wave conditions Bennetts et al. [2015]. A loose mooring was applied to avoid free drift. Tests were also conducted with edge barriers around the floe (as in Montiel et al. [2013b], Yiew et al. [2016], Nelli et al. [2017]; see Figs. 1c,e).

Irregular waves were generated by imposing a JONSWAP spectrum at the wave-maker to model the spectral energy density in the frequency domain and a $\cos^N(\vartheta)$ directional distribution, where N is the directional spreading coefficient and ϑ the wave direction. Random phases uniformly distributed within the interval $[0, \pi)$ and random amplitudes distributed according to a Rayleigh distribution were used when converting spectral energy into piston displacements. The JONSWAP spectrum had peak wave period $T_p = 0.8$ s and peak enhancement factor $\gamma = 3$. Two incident wave field configurations of different strength were tested with significant wave heights $H_s = 4\sqrt{m_0} = 0.032$ m and 0.048 m (where m_0 is the spectral variance). These configurations define a peak wave steepness (a parameter controlling wave dynamics, wave breaking and wave-induced loads Onorato et al. [2009], Toffoli et al. [2010], Alberello et al. [2018], Fadaeiazar et al. [2020]), corresponding to $\varepsilon_p = \pi H_s / L_{w,p} = 0.10$ and 0.15 respectively, where $L_{w,p} \approx L_f$ is the wavelength associated to the peak period through the linear dispersion relation Holthuijsen [2010]. The directional spreading coefficient was set to $N = 100$ to model a unidirectional wave fields and $N = 10$ for a realistic directional sea state Onorato et al. [2009], noting that N switches naturally to a wavelength dependent function after generation Fadaeiazar et al. [2020]. Regular wave fields with wave periods 0.6 s, 0.8 s and 1 s, and different steepness were also tested, and results were reported by Bennetts et al. [2015] although not for cases using edge barriers.

Capacitance gauges monitored the water surface elevation at 128 Hz sampling frequency and ≈ 0.1 mm accuracy. One gauge was deployed 1 m in front of the floe to capture the incident and reflected waves. In the lee of the floe, 3 gauges were deployed every metre to track the transmitted wave field. At 2 m from the rear edge of the floe, a 6-gauge array, arranged as a pentagon of radius of 0.25 m (Fig. 1a), was deployed to measure directional properties. Each incident wave field was tested for all artificial floe configurations (i.e. without and with edge barriers). In addition. benchmark tests were conducted for the incident wave fields in the absence of a floe. For irregular waves, 40-minute time series were recorded to ensure enough data for statistically stable estimates of the wave spectrum, noting that spectral density functions measured in the basin compare well with the input counterpart (see Supplementary Fig. 1), despite some differences in the upper tail. For regular waves, only 5-minute time series were measured due to their deterministic nature.

2.2 Wave transmission in the wavelength-direction domain

Fig. 2 shows the spectral densities of the steepness (ε; a,b,d,e) and the transmission coefficient $\mathcal{T}_{2D}(L_w, \vartheta) = a_{out}(L_w, \vartheta)/a_{in}(L_w, \vartheta)$, i.e. the ratio of transmitted mode amplitudes (a_{out}) to the incident counterparts (a_{in}) with the amplitude being estimated from the spectral energy $E(L_w, \vartheta)$ as $a(L_w, \vartheta) = \sqrt{2E(L_w, \vartheta)\Delta L_w\, \Delta\vartheta}$ (c,f), for the steepest irregular incident wave field ($\varepsilon_p = 0.15$) and for unidirectional ($N = 100$; a,b,c) and directional ($N = 10$; d,e,f) cases. For the steepness, incident (a,d) and transmitted (for a floe without barriers; b,e) spectra are shown. The directional spectral density function is reconstructed with a wavelet directional method Donelan et al. [1996], using time series from the 6-gauge array. The process is applied to windows of 256 data points with 50% overlap and an ensemble average is computed.

For the unidirectional incident wave field (Fig. 2a), energy is concentrated in a narrow directional band ($-10^\circ < \vartheta < 10^\circ$), where the spectral components are steep and experience considerable energy loss during floe interactions Toffoli et al. [2015], with $< 20\%$ of their energy being transmitted (Fig. 2c). The dissipation results in substantial flattening of the spectral shape (Fig. 2b).

For the directional incident wave field (Fig. 2d), the energy is spread across a wide range of directions ($-60^\circ < \vartheta < 60^\circ$). The spectral peak is less sharp and modes carry less steepness than the unidirectional case ($\approx 40\%$ less at the peak), making wave–floe interactions less vigorous. Major energy loss occurs for modes with high steepness ($\varepsilon > 0.035$) over $0.8 < L_w/L_f < 1.4$ and $-10^\circ < \vartheta < 10^\circ$ (Fig. 2f). Transmission increases with angle of propagation for $|\vartheta| > 10^\circ$, as mode steepness decays. The non-uniform transmission rate smooths the spectral peak (Fig. 2e) without altering the spectral density at oblique directions, resulting in an increase of directional spreading.

Incident wave components that do not interact directly with the floe may be present in the transmitted field due to diffraction (in both unidirectional and directional sea states) or reflection from the side walls (in directional sea states), producing directional focusing and, hence, increasing the wave amplitude. Indeed, a weak increasing trend of wave

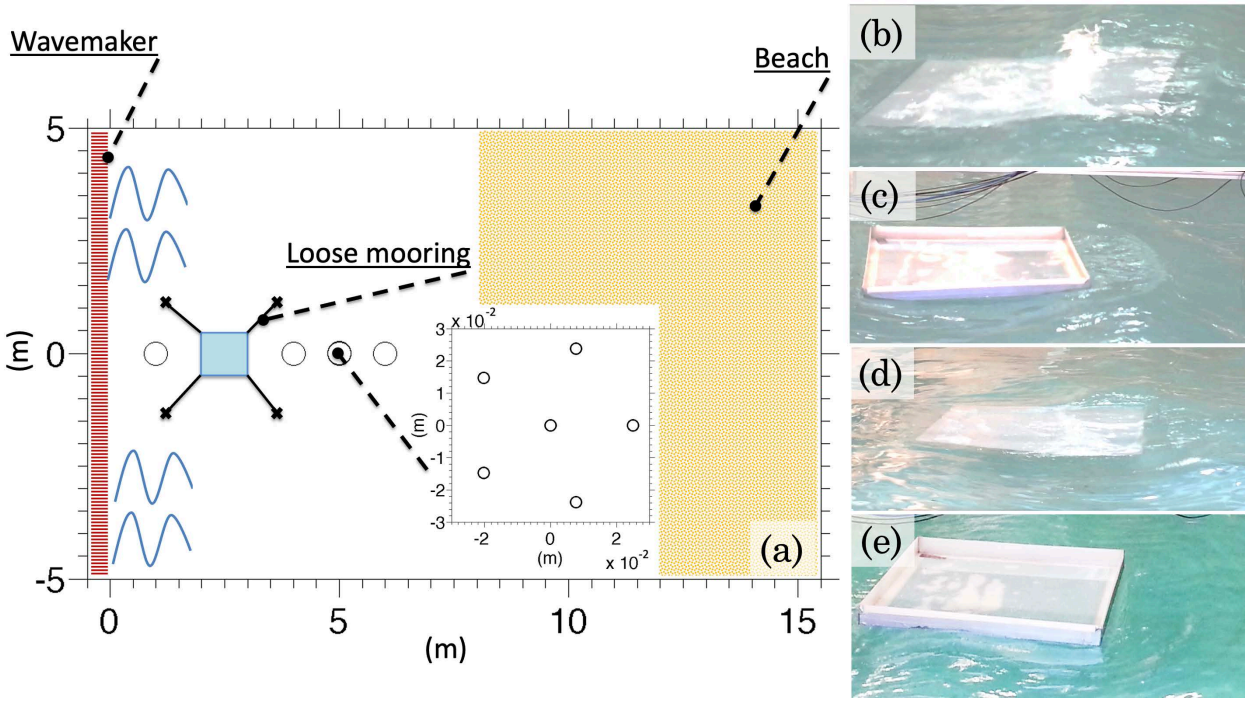

Figure 1: Experimental set-up (a) and snapshots of experiments irregular incident waves with $\varepsilon_p = 0.15$: unidirectional tests ($N = 100$) without (b) and with (c) edge barrier; directional tests ($N = 10$) without (d) and with (e) edge barrier.

energy is reported with distance from the floe (see Supplementary Fig. 2) for both undirectional and directional sea states. Nevertheless, the gain reported at the position of the 6-gauge array is $< 3\%$ relative the measurements at the closest gauge and, hence, it can be considered negligible.

2.3 Transmission coefficient

Fig. 3 shows the transmission coefficient, $\mathcal{T}$, i.e. the average, direction-integrated version of $\mathcal{T}_{2D}$, as a function of normalised wavelength, and includes error bars equivalent to one standard deviation from the ensembles to benchmark uncertainties. Results are shown for all unidirectional ($N = 100$; a,b) and directional ($N = 10$; c,d) incident wave fields, and the least energetic ($\varepsilon_p = 0.10$; a,c) and most energetic ($\varepsilon_p = 0.15$; b,d) cases. Results are also included for regular wave tests with steepness consistent with steepness at the spectral peak and, thus, differ between the left- and right-hand panels, along with 2D linear model predictions Bennetts et al. [2007], which are identical for all panels.

For the unidirectional and least energetic incident wave field ($N = 100$ and $\varepsilon_p = 0.1$; Fig. 3a), the transmission coefficient increases almost monotonically with wavelength, in quantitative agreement with regular wave tests, and full transmission is reached for approximately $L_w/L_f > 1.8$. Overwash was observed during the tests, but its effect on transmission is minor, as substantiated by the generally good agreement with linear theory and tests with barriers, for which transmission is $< 10\%$ greater than tests without barriers.

Broadening the directional spreading ($N = 10$; Fig. 3c) does not have a notable effect for $L_w/L_f > 0.8$, as indicated by the agreement with regular wave tests and linear theory. For $L_w/L_f < 0.8$, the transmission coefficient is $\approx 25\%$ greater than in the unidirectional case, which is attributed to the floe slamming on the water surface, generating high-frequency wave modes (visible in Figs. 1d–e for $\varepsilon_p = 0.15$), as noted previously by Bennetts et al. [2015], Nelli et al. [2017]. The transmission coefficient for the floe with barriers is $< 5\%$ greater than the floe without barrier.

Wave-floe interactions are most intense for the unidirectional and most energetic incident wave field ($N = 100$ and $\varepsilon_p = 0.15$; Fig. 3b). The interactions are characterised by intense overwash (Fig. 1b), which induces significant breaking dissipation over the floe Nelli et al. [2020]. The transmission coefficient decreases in comparison to the $\varepsilon_p = 0.10$ case over most of the wavelength range ($L_w/L_f > 0.7$). The decrease is greatest for $0.7 < L_w/L_f < 1.3$, which contains the steepest modes of the incident field, with $< 50\%$ of the incident energy being transmitted. The decrease is much smaller for the floe with an edge barrier, and negligible for $L_w/L_f > 1.5$. The decrease, which is not visible in the regular wave data, is attributed to localised wave breaking dissipation at the trailing floe end (Fig. 1c).

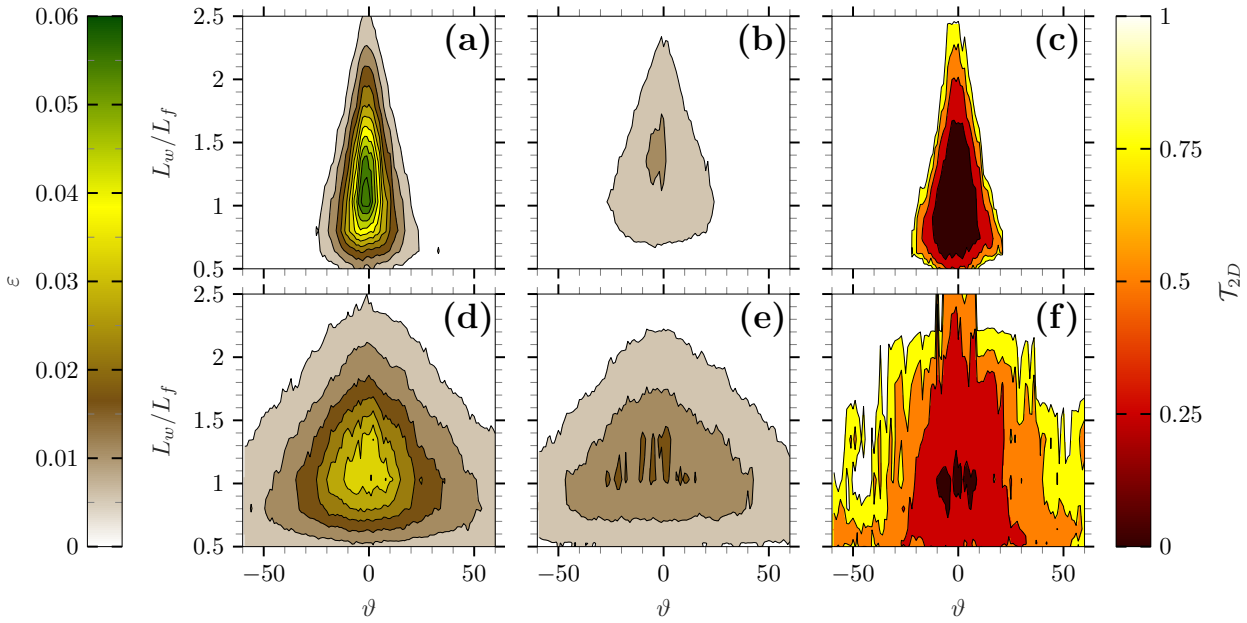

Figure 2: Plots of incident ε (a,d), transmitted ε (b,e) and $\mathcal{T}_{2D}$ (c,f) as function of normalised wavelength and wave direction for unidirectional ($N = 100$) (a,b,c) and directional ($N = 10$) (d,e,f) experiments with $\varepsilon_p = 0.15$.

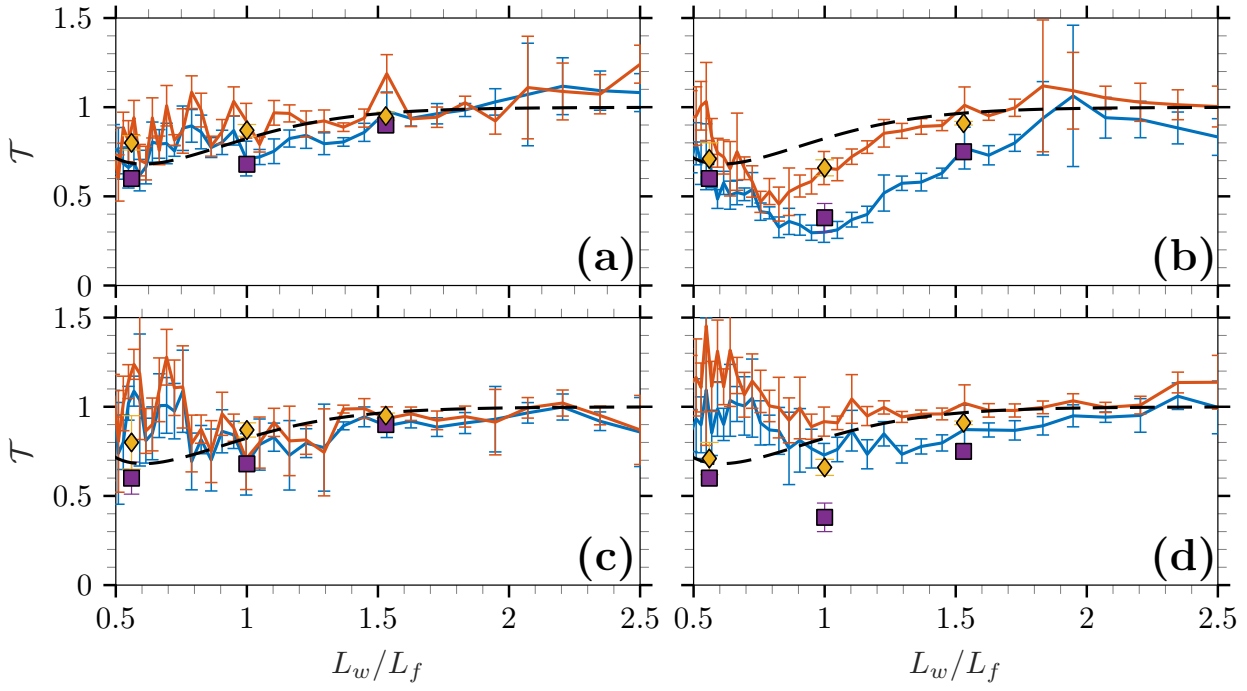

Figure 3: Mean and first standard deviation (error bars) of $\mathcal{T}$ as function of normalised wavelength from experimental results for regular waves with (♦) and without (■) barriers and irregular waves with (—) and without (—) barriers compared to linear theory (– –). The experiments have $N = 100$ and $\varepsilon_p = 0.1$ (a), $N = 100$ and $\varepsilon_p = 0.15$ (b) , $N = 10$ and $\varepsilon_p = 0.1$ (c) and , $N = 10$ and $\varepsilon_p = 0.15$ (d) and regular waves have matching steepness.

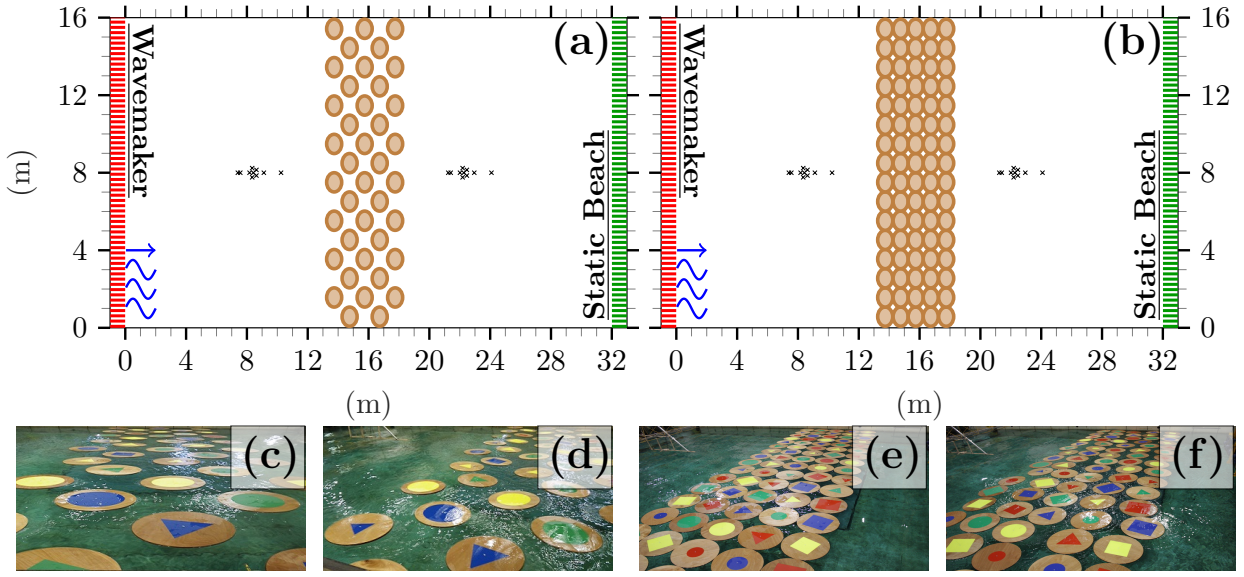

Figure 4: Experimental set-up for low (a) and high (b) concentration basin configurations. Photos taken during low-concentration (c,d) and high-concentration (e,f) array tests.

The transmission coefficients for the irregular wave test agrees with the corresponding transmission coefficients for the regular wave tests.

For the directional incident wave field ($N = 10$; Fig. 1d), the decrease in transmission is much weaker, as the overwash is less intense. There is a pronounced increase in transmission for short wavelengths ($L_w/L_f < 0.9$). It is similar to the increase transmission in the less energetic case (c) and the unidirectional case (b) where the presence of overwash suppresses the increase.

3 Multiple floe experiment

3.1 Experimental set-up

An experiment that investigated the transmission of unidirectional waves through an array of wooden floes was conducted in the Basin de Génie Océanique FIRST wave basin facility, located at Océanide, La Seyne sur Mer, France, for which Bennetts and Williams [2015] reported the regular wave test results. The basin is 16 m wide, 40 m long and filled with fresh water 3.1 m deep. Waves are generated by the wave-maker at the left end of the basin which propagate through the array of floes and are absorbed by an 8 m long static beach at the far end. The water surface elevation to the left and right of the floe array was measured by 10 probes with a 25 Hz sampling frequency.

Two arrays of wooden floes were studied: one with a low concentration of 38% (Fig. 4a,c,d); and another with a high concentration of 77% (Fig. 4b,e,f). Both arrays were composed of circular floes with diameter 0.99 m and thickness 0.033 m. The Young's modulus of the floes was 4 GPa and the density of the floes was 545 kg m^{-3}, which is lower than sea ice and, hence, gives the wooden floes a larger freeboard than ice (and polypropylene) floes. The floes were loosely kept in place using a mooring system that connected the center of the floe to the bottom of the basin. The mooring had a natural period of 12.5 s which was significantly longer than the studied wave periods. The mooring thus allowed the floes to respond with the natural motions predicted by a linear theory of wave action whilst maintaining the array between tests.

Regular and irregular wave tests were conducted for both arrays. The steepness of the regular incident waves were $\varepsilon = 0.02$–0.13, with periods in the range 0.65–2 s for tests that ran for 70 s. The irregular incident waves followed the JONSWAP spectrum with peak enhancement factor $\gamma = 3.3$, peak steepness values $\varepsilon_p = 0.02$–0.08 and peak periods of 0.8 s, 1.4 s and 2 s for tests that ran for 6.5 minutes (comparison of measured wave spectra and target wave spectra provided in Supplementary Fig. 1). All incident regular wave periods and irregular wave peak periods had corresponding calibration tests where no wooden floes were present.

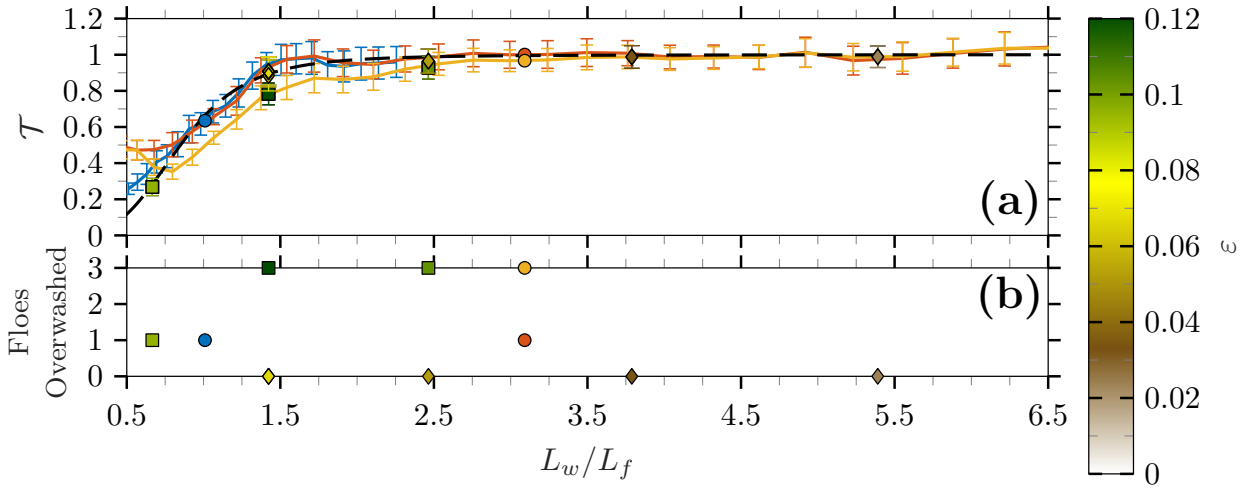

Figure 5: Mean and standard deviation (error bars) of $\mathcal{T}$ as function of normalised wavelength for low-concentration experiments (a) for regular waves where overwash was (■) and was not (♦) observed (colored by ε) and irregular waves experiments with $\varepsilon_p = 0.06$ (—), $\varepsilon_p = 0.04$ (—), $\varepsilon_p = 0.08$ (—) with $L_{w,p}$ shown (●). Observations of number of floes overwashed during experiments (b) where irregular waves are plotted using $L_{w,p}$.

3.2 Low-concentration array

Fig. 5a shows the transmission coefficient at each mode, i.e. $\mathcal{T}(L_w) = a_{out}(L_w)/a_{in}(L_w)$, for all tests (regular and irregular) using the low-concentration array. The wave amplitude for each mode ($a(L_w)$) was estimated from the spectral energy $E(L_w)$ using $a(L_w) = \sqrt{2E(L_w)\Delta L_w}$. The spectral energy $E(L_w)$ was measured from the time series of each transmitted probe by Fourier analysis and averaged over the probes to produce the mean transmitted amplitude for the test (a_{out}) and the corresponding incoming amplitude (a_{in}) from the calibration test, with the error bars denoting a standard deviation between probes Bennetts and Williams [2015].

Predictions from a 2D linear attenuation model Bennetts and Squire [2012] are included as benchmarks. Fig. 5b provides experimental observations of the number of floes overwashed in the direction of wave propagation for each test. Examples of observed number of floes overwashed can be found in Supplementary Fig. 3. In the low-concentration array, the maximum number of floes in the direction of wave propagation is 3, so 3 floes overwashed means all floes in the array were overwashed during the test. In the low-concentration array, no floe–floe collisions were observed and so wave attenuation is attributed to scattering and dissipation in the floe–wave interaction.

The transmission coefficients for the irregular wave tests with $\varepsilon_p = 0.04$ and 0.06 agree well for $L_w/L_f > 0.8$, and also with the low steepness regular wave tests ($\varepsilon < 0.1$) where overwash occurred at most up to one floe deep into the array (Fig. 4c) and the linear model predictions. The agreement indicates that wave transmission through the array is a linear scattering process, and not significantly affected by dissipation due to, for example, overwash. For shorter waves ($L_w/L_f < 0.8$), the agreement between the low steepness irregular wave tests ceases, and both tests have larger $\mathcal{T}$-values than predicted by the linear model, which indicates some transfer of wave energy to shorter wavelengths as observed for the single floe tests in §2. The transfer is most noticeable in the $\varepsilon_p = 0.04$ test, which is likely because the short wavelengths are further from the incident peak wavelength and, thus, had relatively low incident energy.

The irregular wave fields for the $\varepsilon_p = 0.08$ and $\varepsilon_p = 0.04$ tests have the same peak period. The larger steepness results in overwash of all floes in the array and a reduction in $\mathcal{T}$ of up to 16%, due to dissipation. The transmission coefficient agrees with the high steepness regular wave tests ($\varepsilon > 0.1$, where overwash was observed for all floes in the array; Fig. 4d), which is likely because the steepness of the regular waves are comparable to the steepness of the corresponding components of the irregular field, and is not expected to hold in general, as overwash and other dissipative processes are nonlinear Nelli et al. [2020], Skene and Bennetts [2021]. The transmission coefficient reduction is most significant for $0.75 < L_w/L_f < 3.5$. For $L_w/L_f > 3.5$ the reduction is negligible, and for $L_w/L_f < 0.75$ there is evidence of energy transfer, as for the lower steepness tests.

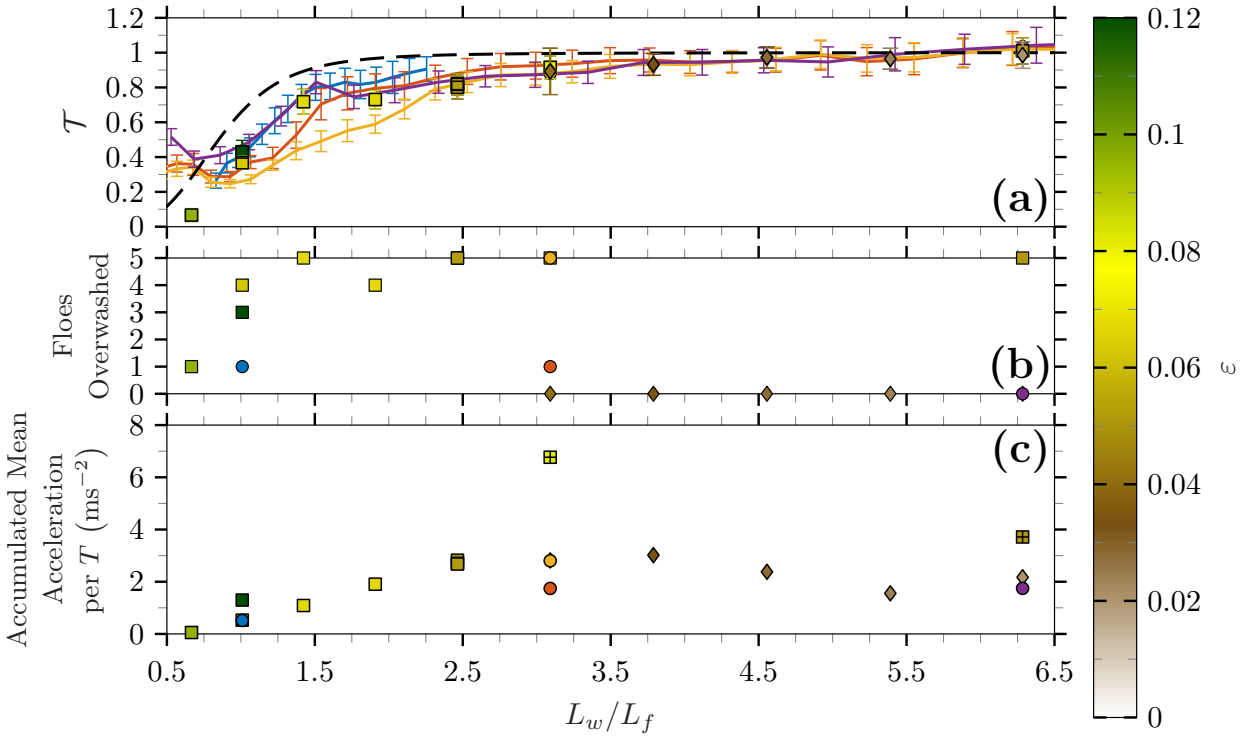

Figure 6: Plots in Fig. 5 repeated for high-concentration experiments with additional irregular wave experiment with $\varepsilon_p = 0.02$ (—). Additional panel showing accumulated mean acceleration per wave period (peak period for irregular waves) from collisions (c) with experiments where the acceleration of one or multiple collisions saturated the signal (+).

3.3 High-concentration array

Fig. 6a–b is identical to Fig. 5a–b but for the high-concentration array with examples of observed number of floes overwashed in Supplementary Fig. 4. Fig. 6c demonstrates the accumulated mean acceleration due to floe–floe collisions per period measured by accelerometers fixed to floes in the middle column of the array. The accumulated mean acceleration combines the measures of frequency (collisions per period) and strength (mean acceleration for each collision) of collisions, which collectively summarise the collision behaviour Bennetts and Williams [2015].

Fig. 6a shows that transmission for the high-concentration array tests are below the linear model predictions, except for $L_w/L_f < 0.75$. For most wavelengths, the measured transmission values are bounded above by the irregular wave experiment with $\varepsilon_p = 0.06$ and below by $\varepsilon_p = 0.08$. From the overwash observations and collision measurements (Fig. 6b–c), the bounding experiments correspond to weak collisions and minimal overwash ($\varepsilon_p = 0.06$; Fig. 4e) and strong collisions and total overwash ($\varepsilon_p = 0.08$; Fig. 4f). Therefore, the reduction in transmission is correlated with the strength of overwash and collisions Yiew et al. [2017], Nelli et al. [2017], noting that dissipation characteristics differ from the low-concentration tests, where no collisions occurred. Further, floe–floe collisions drive overwash of floes, as demonstrated by the incoming waves for which overwash was observed in the high-concentration array but not in the low-concentration array. The effect of dissipation in the experiments is most evident for $0.75 < L_w/L_f < 5.5$, i.e. collision-driven dissipation affects longer wave components. Energy transfer is again inferred for $L_w/L_f < 0.75$. The addition of collision-driven dissipation alters the shape of the transmission curves, which can be seen by comparing the irregular wave tests with the same peak period and different steepness ($\varepsilon_p = 0.04$ and $\varepsilon_p = 0.08$), and contrasts with the effect without collisions (Fig. 5a).

4 Discussion and conclusions

Two independent experimental campaigns in 3D wave basins have been revisited, for which irregular wave tests were conducted but not previously reported. One experiment tested irregular waves, including directional spreading, with two peak steepness values comparable to storm and polar cyclone conditions, interacting with a single square polypropylene floe, with length close to the dominant wavelength (scattering regime). For storm conditions, wave–floe interactions

were relatively weak, allowing $> 80\%$ of energy to be transmitted for both unidirectional and directional waves. Overwash was observed but was not found to affect wave transmission, which is consistent with linear model predictions and regular wave tests. For cyclone-like conditions, wave–floe interactions and overwash were vigorous, forcing intense breaking dissipation to occur on the floe, especially in unidirectional waves, where $< 50\%$ of the incident energy is transmitted. The unidirectional irregular wave and regular wave tests agreed well and both were overpredicted by the linear model, which does not capture overwash dissipation. Directional spreading reduced the steepness of individual wave components, decreasing dissipation due to overwash and, hence, enhancing transmission.

The second experiment used arrays of wooden floes. Transmission of unidirectional irregular waves through low- and high-concentration floe arrays were tested at a range of peak periods and peak wave steepnesses spanning gentle to storm-like conditions. For the low-concentration array, transmission of gentle regular and irregular incident waves were predicted accurately by a linear model. Transmission decreased for storm-like waves, due to dissipation effects correlated with the number of floes overwashed. For the high-concentration array, agreement was found between irregular and regular wave tests but transmission was below model predictions, even for gentle steepness, which correlated with the strength of floe–floe collisions and overwash. The high-concentration array demonstrated collision-driven overwash, in contrast to current overwash models where overwash is due solely to individual floe interactions with large (steep) waves Skene et al. [2015], Skene and Bennetts [2021], Pitt et al. [2022].

The experiments have key differences beyond the number of floes involved in the tests, such as the material densities used for the floes, which resulted in (unrealistically) large freeboard in the multiple floe tests, and, hence, different overwash onset thresholds. However, both experiments identify that (i) overwash, whether forced by wave impact on a single floe or collisions in an array of floes, is a driver for wave attenuation, and (ii) across the full wave spectrum, overwash-driven dissipation is the most effective for wavelengths comparable with floe length. The shared findings from two independent experiments are evidence of their robustness. Further, there is good agreement between irregular and regular wave tests, especially when undirectional propagation is assumed. Directional spreading, nonetheless, creates inconsistencies with regular tests, due to a reduced overwash. Knowledge of the directional wave spectrum is therefore important to achieve a more accurate estimation of wave–ice interaction processes in realistic oceanic conditions.

Contemporary global wave models compute wave attenuation in the MIZ with dissipation terms based on friction or viscoelastic processes Ardhuin et al. [2018], Iwasaki and Otsuka [2021] and linear scattering Meylan and Bennetts [2018], Perrie and Meylan [2022], but exclude collisions and overwash due, in part, to a lack of direct in-situ observations. Considering that floe sizes in the MIZ (10–100 m) are comparable with wavelengths of dominant (i.e. most energetic) wave components ($\approx$ 25-350 m Stopa et al. [2016], Derkani et al. [2021]), it is perhaps unsurprising that model predictions are reported to over estimate wave heights in the Arctic MIZ Ardhuin et al. [2018]. With large waves reported in high-concentration MIZs more than 50 km from the edge Vichi et al. [2019], Alberello et al. [2021], Kohout et al. [2020], an accurate estimation of wave attenuation in the the MIZ is important to evaluate sea ice dynamics. The challenge is to design new field studies and develop detailed models to resolve these mechanisms, in order to allow a generalization of the attenuation rate.

Data accessibility

Data can be downloaded at `https://doi.org/10.5281/zenodo.6332923`.

Author contribution

AT, LGB and JP conceived the manuscript; AT and AA designed and carried out the single floe experiment; LGB co-designed the multiple floe experiment; AT, LGB and JP analysed experimental data. All authors contributed to writing the manuscript.

Competing interests

The authors declare that they have no competing interests.

Funding

The authors acknowledge support from the Australian Research Council grant DP200102828. LGB is supported by the Australian Research Council grant FT190100404. The multiple floe experiment was funded by the Collaborative & Innovative Technology Program in Exploration and Production of Hydrocarbons, with major sponsors Total, Saipem and Doris Engineering.

Acknowledgements

Experiments with a single plate at the University of Plymouth were supported by the School of Marine Science and Engineering; the authors thank Peter Arber for technical support during the these experiments. Experiments at Océanide, La Seyne Sur Mer were co-designed and conducted by Francois Pétrié, Vincent Lafon, Thierry Rippol and Alexandre Cinello.

References

A. Alberello, A. Chabchoub, J. P. Monty, F. Nelli, J. H. Lee, J. Elsnab, and A. Toffoli. An experimental comparison of velocities underneath focussed breaking waves. *Ocean Eng.*, 155:201–210, 2018.

A. Alberello, L. G. Bennetts, P. Heil, C. Eayrs, M. Vichi, K. MacHutchon, M. Onorato, and A. Toffoli. Drift of pancake ice floes in the winter Antarctic marginal ice zone during polar cyclones. *J. Geophys. Res.—Oceans*, 125(3): e2019JC015418, 2020.

A. Alberello, A. Dolatshah, L. G. Bennetts, M. Onorato, F. Nelli, and A. Toffoli. A physical model of wave attenuation in pancake ice. *Int. J. Offshore Polar Eng.*, 31(03):263–269, 2021.

A. Alberello, L. G. Bennetts, M. Onorato, M. Vichi, K. MacHutchon, C. Eayrs, B. Ntamba Ntamba, A. Benetazzo, F. Bergamasco, F. Nelli, R. Pattani, H. Clarke, I. Tersigni, and A. Toffoli. Three-dimensional imaging of waves and floe sizes in the marginal ice zone during an explose cyclone. *arXiv:2103.08864*, 2022. URL `https://arxiv.org/pdf/2103.08864`.

F. Ardhuin, G. Boutin, J. Stopa, F. Girard-Ardhuin, C. Melsheimer, J. Thomson, A. Kohout, M. Doble, and P. Wadhams. Wave attenuation through an Arctic marginal ice zone on 12 october 2015: 2. Numerical modeling of waves and associated ice breakup. *J. Geophys. Res.—Oceans*, 123(8):5652–5668, 2018.

W. Bai, T. Zhang, and D. J. McGovern. Response of small sea ice floes in regular waves: A comparison of numerical and experimental results. *Ocean Eng.*, 129:495–506, 2017.

L. G. Bennetts and T. D. Williams. Wave scattering by ice floes and polynyas of arbitrary shape. *J. Fluid Mech.*, 662: 5–35, 2010.

L. G. Bennetts and T. D. Williams. Water wave transmission by an array of floating discs. *Proc. Roy. Soc. A*, 471(2173): 20140698, 2015.

L. G. Bennetts, N. R. T. Biggs, and D. Porter. A multi-mode approximation to wave scattering by ice sheets of varying thickness. *J. Fluid Mech.*, 579:413–443, 2007.

L. G. Bennetts, A. Alberello, M. H. Meylan, C. Cavaliere, A. V. Babanin, and A. Toffoli. An idealised experimental model of ocean surface wave transmission by an ice floe. *Ocean Model.*, 96:85–92, 2015.

L. G. Bennetts, S. O'Farrell, and P. Uotila. Impacts of ocean-wave-induced breakup of Antarctic sea ice via thermodynamics in a stand-alone version of the CICE sea-ice model. *Cryosphere*, 11(3):1035–1040, 2017.

Luke G. Bennetts and Vernon A. Squire. On the calculation of an attenuation coefficient for transects of ice-covered ocean. *Proc. Roy. Soc. A*, 468(2137):136–162, 2012.

J. Brouwer, A. D. Fraser, D. J. Murphy, P. Wongpan, A. Alberello, A. Kohout, C. Horvat, S. Wotherspoon, R. A Massom, J. Cartwright, and G. D. Williams. Altimetric observation of wave attenuation through the antarctic marginal ice zone using icesat-2. *The Cryosphere Discussions*, pages 1–40, 2021.

M. Dai, H. H. Shen, M. A. Hopkins, and S. F. Ackley. Wave rafting and the equilibrium pancake ice cover thickness. *J. Geophys. Res.—Oceans*, 109(C7):C07023, 2004.

M. H. Derkani, A. Alberello, F. Nelli, L. G. Bennetts, K. G. Hessner, K. MacHutchon, K. Reichert, L. Aouf, S. Khan, and A. Toffoli. Wind, waves, and surface currents in the Southern Ocean: Observations from the Antarctic circumnavigation expedition. *Earth Syst. Sci. Data*, 13(3):1189–1209, 2021.

A. Dolatshah, F. Nelli, L. G. Bennetts, A. Alberello, M. H. Meylan, J. P. Monty, and A. Toffoli. Hydroelastic interactions between water waves and floating freshwater ice. *Phys. Fluids*, 30(9):091702, 2018.

M. A. Donelan, W. M. Drennan, and A. K. Magnusson. Nonstationary analysis of the directional properties of propagating waves. *J. Phys. Oceanog.*, 26(9):1901–1914, 1996.

D. Dumont. Mini review on marginal ice zone dynamics and breakup and implications for other science areas. *Philos. T. Roy. Soc. A*, This issue(submitted), 2022.

E. Fadaeiazar, J. Leontini, M. Onorato, T. Waseda, A. Alberello, and A. Toffoli. Fourier amplitude distribution and intermittency in mechanically generated surface gravity waves. *Phys. Rev. E*, 102(1):013106, 2020.

Kenneth M. Golden, Luke G. Bennetts, Elena Cherkaev, Ian Eisenman, Daniel Feltham, Christopher Horvat, Elizabeth Hunke, Christopher Jones, Donald K. Perovich, Pedro Ponte-Castaneda, Courtenay Strong, Deborah Sulsky, and Andrew J. Wells. Modeling sea ice. *Not. Am. Math. Soc.*, 67(10):1535–1555, 2020.

Shen H. H. Wave-in-ice: Theoretical bases and field observations. *Philos. T. Roy. Soc. A*, This issue(submitted), 2022.

Agnieszka Herman, Sukun Cheng, and Hayley H Shen. Wave energy attenuation in fields of colliding ice floes–part 2: A laboratory case study. *The Cryosphere*, 13(11):2901–2914, 2019.

L. H. Holthuijsen. *Waves in oceanic and coastal waters*. Cambridge University Press, 2010.

C. Horvat. review on marginal ice zone floe size distributions and implications for other science areas. *Philos. T. Roy. Soc. A*, This issue(submitted), 2022.

S. Iwasaki and J. Otsuka. Evaluation of wave-ice parameterization models in WAVEWATCH III® along the coastal area of the Sea of Okhotsk during winter. *Front. Mar. Sci.*, 2021.

A. L. Kohout, M. J. M. Williams, S. M. Dean, and M. H. Meylan. Storm-induced sea-ice breakup and the implications for ice extent. *Nature*, 509(7502):604, 2014.

A. L. Kohout, M. Smith, L. A. Roach, G. Williams, F. Montiel, and M. J. M. Williams. Observations of exponential wave attenuation in Antarctic sea ice during the PIPERS campaign. *Ann. Glaciol.*, 61(82):196–209, 2020.

D. Masson and P. LeBlond. Spectral evolution of wind-generated surface gravity waves in a dispersed ice field. *J. Fluid Mech.*, 202:111–136, 1989.

D. J. McGovern and W. Bai. Experimental study on kinematics of sea ice floes in regular waves. *Cold Reg. Sci. Technol.*, 103:15–30, 2014.

M. H. Meylan, V. A. Squire, and C. Fox. Towards realism in modeling ocean wave behavior in marginal ice zones. *J. Geophys. Res.*, 102(C10):22981–22991, 1997.

M. H. Meylan, L. G. Bennetts, C. Cavaliere, A. Alberello, and A. Toffoli. Experimental and theoretical models of wave-induced flexure of a sea ice floe. *Phys. Fluids*, 27(4):041704, 2015a.

M. H. Meylan, L. G. Bennetts, J. E. M. Mosig, W. E. Rogers, M. J. Doble, and M. A. Peter. Dispersion relations, power laws, and energy loss for waves in the marginal ice zone. *J. Geophys. Res.—Oceans*, 123(5):3322–3335, 2018.

Michael H. Meylan and Luke G. Bennetts. Three-dimensional time-domain scattering of waves in the marginal ice zone. *Philos. T. Roy. Soc. A*, 376(2129):20170334, 2018.

Michael H. Meylan, Lucas J. Yiew, Luke G. Bennetts, Benjamin J. French, and Giles A. Thomas. Surge motion of an ice floe in waves: comparison of a theoretical and an experimental model. *Ann. Glaciol.*, 56(69):155–159, 2015b.

F. Montiel, L. G. Bennetts, V. A. Squire, F. Bonnefoy, and P. Ferrant. Hydroelastic response of floating elastic discs to regular waves. Part 2. Modal analysis. *J. Fluid Mech.*, 723:629–652, 2013a.

F. Montiel, F. Bonnefoy, P. Ferrant, L. G. Bennetts, V. A. Squire, and P. Marsault. Hydroelastic response of floating elastic discs to regular waves. Part 1. Wave basin experiments. *J. Fluid Mech.*, 723:604–628, 2013b.

F. Nelli, L. G. Bennetts, D. M. Skene, J. P. Monty, J. H. Lee, M. H. Meylan, and A. Toffoli. Reflection and transmission of regular water waves by a thin, floating plate. *Wave Motion*, 70:209–221, 2017.

F. Nelli, L. G. Bennetts, D. M. Skene, and A. Toffoli. Water wave transmission and energy dissipation by a floating plate in the presence of overwash. *J. Fluid Mech.*, 889, 2020.

M. Onorato, L. Cavaleri, S. Fouques, O. Gramstad, P. A. E. M. Janssen, J. Monbaliu, A. R. Osborne, C. Pakozdi, M. Serio, C. T. Stansberg, A. Toffoli, and K. Trulsen. Statistical properties of mechanically generated surface gravity waves: A laboratory experiment in a three-dimensional wave basin. *J. Fluid Mech.*, 627:235–257, 2009.

Mark D. Orzech, Fengyan Shi, Jayaram Veeramony, Samuel Bateman, Joseph Calantoni, and James T. Kirby. Incorporating floating surface objects into a fully dispersive surface wave model. *Ocean Model.*, 102:14–26, 2016.

Giulio Passerotti, Luke G Bennetts, Franz von Bock und Polach, Alberto Alberello, Otto Puolakka, Azam Dolatshah, Jaak Monbaliu, and Alessandro Toffoli. Interactions between irregular wave fields and sea ice: A physical model for wave attenuation and ice breakup in an ice tank. *J. Phys. Oceanogr.*, 2022.

W. Perrie and M. H. Meylan. Representations of wave scattering and attenuation due to sea ice in global spectral wave models. *Philos. T. Roy. Soc. A*, This issue(submitted), 2022.

M. A. Peter, M. H. Meylan, and H. Chung. Wave scattering by a circular elastic plate in water of finite depth: A closed form solution. *Int. J. Offshore Polar Eng.*, 14(2):81–85, 2004.

Jordan P. A Pitt, Luke G. Bennetts, Michael H. Meylan, Robert A. Massom, and Alessandro Toffoli. Model predictions of wave overwash extent into the marginal ice zone. 2022. doi:10.48550/ARXIV.2204.01891. URL `https://arxiv.org/abs/2204.01891`.

Kaj Riska. Ice edge failure process and modelling ice pressure. *Philos. T. Roy. Soc. A*, 376(2129):20170340, 2018.

D. M. Skene, L. G. Bennetts, M. H. Meylan, and A. Toffoli. Modelling water wave overwash of a thin floating plate. *J. Fluid Mech.*, 777, 2015.

David M. Skene and Luke G. Bennetts. A transition-loss theory for waves reflected and transmitted by an overwashed body. *SIAM J. Appl. Math.*, 81(3):834–852, 2021.

Vernon A. Squire. Past, present and impendent hydroelastic challenges in the polar and subpolar seas. *Philos. T. Roy. Soc. A*, 369(1947):2813–2831, 2011.

Vernon A Squire, John P Dugan, Peter Wadhams, Philip J Rottier, and Antony K Liu. Of ocean waves and sea ice. *Ann. Rev. Fluid Mech.*, 27:115–168, 1995.

J. E. Stopa, F. Ardhuin, and F. Girard-Ardhuin. Wave climate in the arctic 1992–2014: Seasonality and trends. *The Cryosphere*, 10(4):1605–1629, 2016.

J. Thomson. Wave propagation in the marginal ice zone: Connections and feedbacks within the air-ice-ocean system. *Philos. T. Roy. Soc. A*, This issue(submitted), 2022.

J. Thomson and W. E. Rogers. Swell and sea in the emerging Arctic ocean. *Geophys. Res. Lett.*, 41(9):3136–3140, 2014.

G. W. Timco and W. F. Weeks. A review of the engineering properties of sea ice. *Cold Reg. Sci. Technol.*, 60:107–129, 2010.

A. Toffoli, A. Babanin, M. Onorato, and T. Waseda. Maximum steepness of oceanic waves: Field and laboratory experiments. *Geophys. Res. Lett.*, 37(5), 2010.

A. Toffoli, L. G. Bennetts, M. H. Meylan, C. Cavaliere, A. Alberello, J. Elsnab, and J. P. Monty. Sea ice floes dissipate the energy of steep ocean waves. *Geophys. Res. Lett.*, 42(20):8547–8554, 2015.

M. Vichi, C. Eayrs, A. Alberello, A. Bekker, L. G. Bennetts, D. Holland, E. de Jong, W. Joubert, K. MacHutchon, G. Messori, J. F. Mojica, M. Onorato, C. Saunders, S. Skatulla, and A. Toffoli. Effects of an explosive polar cyclone crossing the Antarctic marginal ice zone. *Geophys. Res. Lett.*, 46(11):5948–5958, 2019.

F. von Bock Und Polach, M. Klein, and M. Hartmann. A new model ice for wave–ice interaction. *Water*, 13(23):3397, 2021.

Ruixue Wang and Hayley H. Shen. Experimental study on surface wave propagating through a grease–pancake ice mixture. *Cold Reg. Sci. Technol.*, 61(2-3):90–96, 2010.

Timothy D. Williams, Luke G. Bennetts, Vernon A. Squire, Dany Dumont, and Laurent Bertino. Wave–ice interactions in the marginal ice zone. Part 1: Theoretical foundations. *Ocean Model.*, 71:81–91, 2013a.

Timothy D. Williams, Luke G. Bennetts, Vernon A. Squire, Dany Dumont, and Laurent Bertino. Wave–ice interactions in the marginal ice zone. Part 2: Numerical implementation and sensitivity studies along 1D transects of the ocean surface. *Ocean Model.*, 71:92–101, 2013b.

Timothy D. Williams, Pierre Rampal, and Sylvain Bouillon. Wave–ice interactions in the neXtSIM sea-ice model. *Cryosphere*, 11(5):2117–2135, 2017.

L. J. Yiew, L. G. Bennetts, M. H. Meylan, G. A. Thomas, and B. J. French. Wave-induced collisions of thin floating disks. *Phys. Fluids*, 29(12):127102, 2017.

L.J. Yiew, L.G. Bennetts, M.H. Meylan, B.J. French, and G.A. Thomas. Hydrodynamic responses of a thin floating disk to regular waves. *Ocean Model.*, 97:52–64, 2016.